Journal of Polymers and the Environment
https://doi.org/10.1007/s10924-024-03390-7

ORIGINAL PAPER

A Novel Magnetic and Amino Grafted Chitosan-Based Composite for Efficient Adsorption and Reduction of Cr(VI): Performance and Removal Mechanism

Lixin Huang[1] · Mingen Li[1] · Haiying Lin[1,2] · Qingge Feng[1,2] · Qiuyan Hu[1] · Zixuan Chen[1] · Jiatong Lv[1] · Jia Lin[1] · Lianghong Li[1] · Xianghua Wu[1]

Accepted: 17 August 2024

Abstract

The discharge of industrial wastewater containing Cr(VI) can severely damage the surrounding environment and cause serious threats to human health. Exploring high-performance adsorbents to rapidly remove Cr(VI) could be a popular idea for solving this problem. Herein, a composite (Fe_3O_4@CS-APTMS) was fabricated by using Fe_3O_4 as the core coated with chitosan and then functionalized with APTMS for simultaneous Cr(VI) reduction and adsorption. Although the APTMS grafting and the cross-linking reaction covered the Fe_3O_4@CS-APTMS surface with more obvious folding and wrinkling and blocked the interior pores, the graft-rich amino functional groups could effectively enhance the acidic pH adaptability and the performance of Fe_3O_4@CS-APTMS to achieve an adsorption capacity of 269.54 mg g^{-1} at 298 K and pH 2.0. The primary reaction mechanism involving electrostatic attraction, reduction, and chelation of Cr(VI) has been thoroughly investigated through FTIR, XPS, and DFT analyses. Moreover, the concentration of Cr(VI) (32 mg L^{-1}) in artificial electroplating wastewater substantially decreased to 0.09 mg L^{-1} post-treatment, significantly below China's discharge standard (0.2 mg L^{-1}). Furthermore, the composite demonstrated excellent resistance to disturbances and recyclability. Thus, the synthesized composite emerges as a promising alternative material for efficiently treating chromium-containing electroplating wastewater, underscoring the importance of amino-modified materials in Cr(VI) reduction and detoxification in aquatic environments.

✉ Haiying Lin
linhaiying@gxu.edu.cn

[1] School of Resources, Environment and Materials, Guangxi University, Nanning 530004, China

[2] State Key Laboratory of Featured Metal Materials and Life-cycle Safety for Composite Structures, Guangxi University, Nanning, China

Published online: 30 August 2024

Graphical Abstract

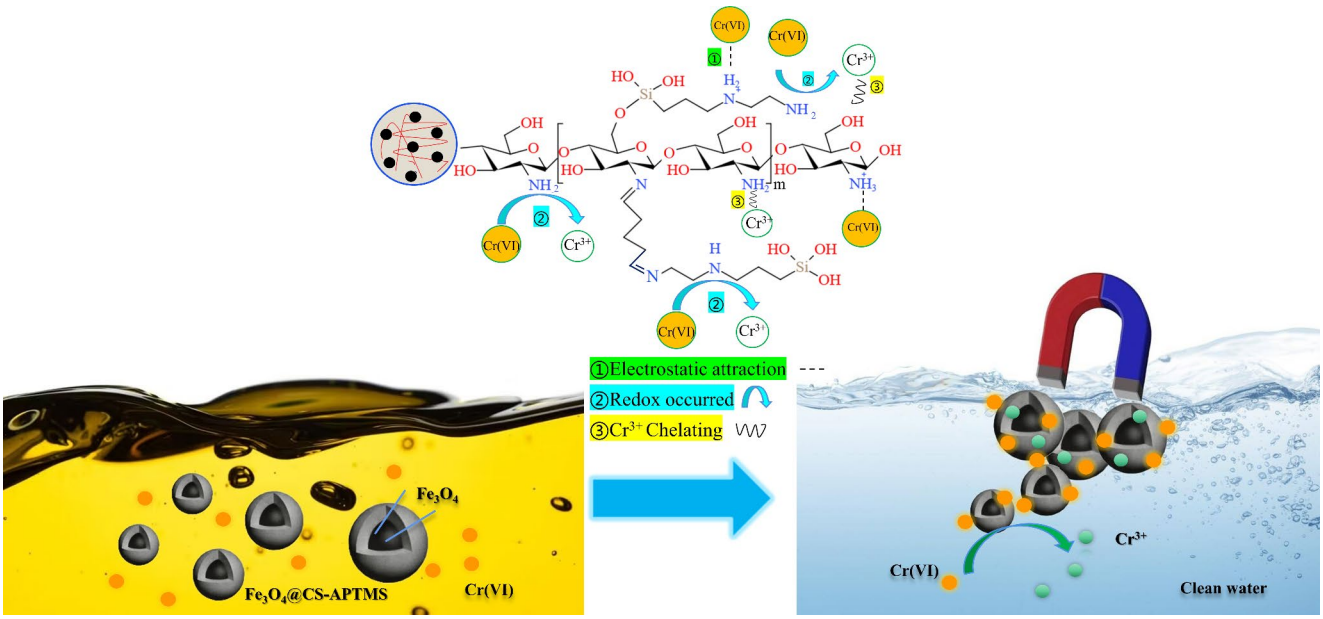

Keywords Amino-modified · Chromium · Chitosan · Adsorption · Reduction · Magnetic composite

Introduction

The wastewater containing high levels of hexavalent chromium (Cr(VI)) was widely found in industries including metal finishing, electroplating, leather processing, and textile dying industry [1]. Discharge of Cr(VI)-containing industrial wastewater into the aquatic environment can harm downstream water sources and pose a potential risk to human health [2]. For example, the Hinkley chromium pollution case in California, the Tokyo chromium pollution case in Japan, and the Nanpan River chromium residue water pollution case in Yunnan province. Owing to its high toxicity, and strong mutagenicity and carcinogenicity [3], the Chinese government restricts the threshold value of Cr(VI) concentration in industrial effluent to be 0.2 mg L^{-1} based on China's "Emission standard of pollutants for electroplating" (GB21900-2008) [4]. Among numerous treatments for treating Cr(VI)-polluted wastewater, the adsorption method is currently the most attractive and effective method due to its wide range of adsorbents, simple operation, ease of recovery, and high efficiency [5, 6]. At present, multiple kinds of material have been synthesized and widely employed in the field of toxic metal removal, such as zeolite [7], clay minerals [8], activated carbon [9], and mesoporous silica [10]. Although these adsorbents are well-developed, they still have limited adsorption performance due to insufficient active groups. High performance is the key point for the material's potential for practical application [11–16]. Hence, it is crucial to develop a novel adsorbent with abundant and approachable functional groups for efficient removal of Cr(VI).

Chitosan(CS) has been widely researched in wastewater treatment due to its appealing attributes, including its non-toxic nature, biodegradability, and a significant number of available groups [17]. However, the raw CS material still has the following defects that need to be addressed. On the one hand, its adsorption capacity was recorded as 102 mg g^{-1} [18], which still requires further improvement. On the other hand, real industrial wastewater containing Cr(VI) has been discovered at a low pH of 2.0–3.0 [1]. In this scenario, the -NH_2 protonation (via acid treatment) of the polymeric chain causes CS to dissolve in wastewater which consequently reduces its inherent adsorption capacity [17].

To overcome these challenges, cross-linking or surface grafting of CS chains using various chemicals can be employed [19]. For example, diethylenetriamine-pentaacetic acid [20], vanillin [21], and poly(acryloyloxyethyltrimethyl ammonium chloride [22], have been used to modify CS to achieve the excellent removal capability of Cr(VI). Moreover, many previous studies gave evidence that the adsorption of mesoporous materials can be effectively enhanced by embedding organic ligands on the surface of mesoporous materials [12, 23–26]. Among various organic modifying agents, 3-aminopropyl trimethoxysilane (APTMS) is a commercially available bifunctional compound that possesses two kinds of functional groups, namely active amino

and hydrolyzable siloxanes. It can graft onto the CS surface via dehydration condensation between siloxanes and hydroxyl groups [27]. However, the chemical crosslinking through APTMS-embedding on CS to overcome acid solubility and enhance adsorption properties of Cr(VI) has not been yet explored.

Moreover, the rapid collection of CS adsorbents in water to prevent secondary pollution is also a concern that needs to be addressed. Magnetic nanoparticles, especially Fe_3O_4 nanoparticles, provide a new thought on account that they can be rapidly collected under the external magnetic field [3].

This study presented a promising novel magnetic chitosan adsorbent utilizing APTMS via Schiff base formation and cross-linking, which can selectively, efficiently, and quickly remove Cr(VI) from acidic wastewater. The main objectives of this study are to (i) probe the effect of solution pH, contact time, initial concentration, temperature, ionic strength, and coexisting ions on the adsorption performance of Fe_3O_4@CS-APTMS toward Cr(VI); (ii) investigate the Cr(VI) adsorption and reduction properties of Fe_3O_4@CS-APTMS; (iii) elucidate the possible mechanisms of Cr(VI) removal by Fe_3O_4@CS-APTMS.

Materials and Methods

Chemicals and Instruments

Some reagents and solvents, for example, sodium hydroxide, ethanol, acetone, potassium dichromate, copper nitrate trihydrate, cadmium nitrate tetrahydrate, lead nitrate, cobalt nitrate, magnesium nitrate hexahydrate, were purchased from Guangdong Guanghua Technology Co., Ltd. The Nano-Fe_3O_4 (purity 99.5%), 3-(2-aminoethyl amino) propyl trimethoxysilane (95% purity, APTMS), Chitosan (95% purity, CS), were obtained from Shanghai Mclean Biochemical Technology Co., Ltd., Shanghai Adamas Chemical Reagent Co. Ltd. and Sigma-Aldrich Ltd, respectively. Hexavalent chromium standard material was purchased from Beijing North Weiye Metrology Technology Research Institute.

The morphology and element distribution of the nanoparticles were characterized by scanning electron microscope (SEM, QUANTA FEG250) and transmission electron microscopy (TEM, FIRTracer-100). Fourier-transformed infrared spectroscopy (FT-IR, Nicolet IS10) was employed to analyze chemical bonds and functional groups. The crystal structure and magnetic properties of the magnetic beads were investigated by an X-ray diffractometer (XRD, Rigaku D/MAX 2500 V) and a vibrating sample magnetometer (VSM, 7410, America). X-ray photoelectron spectroscopy (XPS, Thermo Scientific Nexsa) was used to analyze the crystal structure.

Preparation of Fe_3O_4@CS-APTMS Composites

The preparation process of Fe_3O_4@CS-APTMS is exhibited in Fig. S1. To be specific, 1.0 g CS was dispersed in 50 mL acetic acid aqueous solution (5 wt%) under magnetic stirring; 0.5 g Fe_3O_4 was added and mixed with ultrasound for 15 min to obtain the homogeneous Fe_3O_4@CS solution. Then, 50 mL of NaOH (2 mol L^{-1}) solution was dropwise added into the mixture by a peristaltic pump at a rate of 2 mL min^{-1} to form a magnetic wet gel; they were incubated for more than 30 min and rinsed with ultrapure water for several times. Subsequently, the magnetic wet gel was immersed into 200 mL ultrapure water containing a certain amount of APTMS and 1.5 mL glutaraldehyde (25 wt%) at a fixed temperature for a while. Finally, the Fe_3O_4@CS-APTMS composite was washed and vacuum freeze-dried for 36 h. At the same time, the unmodified Fe_3O_4@CS was prepared without the modification step for comparison.

Batch Adsorption Experiment

Batch experiments were performed in a series of glass vials (40 mL) at 298 K and pH 2.0 except otherwise indicated. The volume of aqueous Cr (VI) solution was maintained at 50 mL, initial Cr(VI) concentration was kept at 200 mg L^{-1}, and Fe_3O_4@CS-APTMS dosage was set as 1.0 g L^{-1}. After reaction for a specified time, the solids were magnetically separated, and the Cr(VI) concentrations in the solution before and after adsorption were measured by the 1,5-Diphenylcarbohydrazide spectrophotometric method using UV–vis spectrophotometer (UV-1800PC) (λ_{max} = 540 nm) [28].

The initial pH of the solutions was controlled from 1 to 11 to study the effect of pH on adsorption. The adsorption experiments were conducted under different dosages of Fe_3O_4@CS-APTMS (0.10 ~ 2.0 g L^{-1}) to ascertain the optimum dosage. In the isotherm experiment, the initial concentration was varied from 50 to 500 mg L^{-1}, the temperature was controlled at 298, 318, and 338 K, and the adsorption interval was 12 h. For the kinetics experiment, the aliquots were withdrawn and filtrated at several time points throughout 720 min for residual Cr(VI) determination. The residual Cr(VI) concentrations were determined by a diphenylcarbazide method (DPC) on a UV–vis spectrophotometer at 540 nm wavelength. Total Cr concentrations in aqueous solution were measured using an inductively coupled plasma emission spectrometer ICP-AES (ICPS-7510, Japan). The content difference between total chromium and Cr(VI) was the concentration of Cr(III). According to the characteristics

of the actual electroplating wastewater, the regeneration experiments were performed at an initial Cr(VI) solution of 50 mg L^{-1} and reacted for 12 h. In this study, simulated electroplating wastewater at pH 2 formulated according to certain industrial electroplating wastewater parameters [29] is shown in Table 1.

Regeneration Studies

According to the characteristics of the actual electroplating wastewater, the adsorbent at 1 g L^{-1} was added to wastewater spiked with 50 mg L^{-1} of Cr(VI) and reacted for 60 min. The Fe_3O_4@CS-APTMS-Cr was separated via magnetic separation and then immersed in 50 mL of 0.01 M NaOH for 15 min, after that the composites were washed several times with water and then freeze-dried. Then the absorbent experienced the next adsorption-desorption cycle.

DFT Calculations

The geometry was calculated by density functional theory (DFT) using the DMol3 module of the Materials Studio (MS) software package. The interaction energy (E_{int}) of Cr(VI) ions adsorption on Fe_3O_4@CS-APTMS was determined using the Generalized gradient approximation (GGA) in conjunction with the Perdew–Burke–Ernzerhof (PBE) exchange-correlation function. We used a simplified model of CS-APTMS to calculate interaction energy with Cr(VI). Cr(VI) predominantly existed as $HCrO_4^-$ in the pH range of 2 to 6. The amine groups were joined by H^+ ions on account that it was protonated in such an acidic environment.

The adsorption properties of the molecule on the Fe_3O_4@CS-APTMS were examined by the interaction energy (E_{int}) with Eq. (1):

$$E_{\text{int}} = E_{A\cdots B} - E_A - E_B \tag{1}$$

where the E_{AB}, E_A, and E_B are the total energies of combinations of A and B, substance A and substance B, respectively. The E_{int} value indicates a strong binding between the adsorbent and the adsorbate.

Data and Statistical Analysis

The samples in batch experiments were conducted in triplicate ($n \geq 3$), and their arithmetic means and standard deviation (SD) were taken as the results. X-correlation graphs were drawn based on the plotting function of Origin 2021b, where column/dispersion symbols indicated the arithmetic mean and error bars indicated the SD. In addition, data from the experiments involving the kinetics and isothermal were linearly fitted by least squares using Origin 2021b, and the arithmetic means of the groups were compared employing comparative analysis. The raw data was transferred before these statistical analyses, the detailed calculation method was described in the corresponding section.

The adsorption capacity (q_e) and removal efficiency (R) were calculated by Eqs. 2 and 3:

$$q_e = (C_0 - C_e)\frac{V}{m} \tag{2}$$

$$R\,(\%) = \frac{C_0 - C_e}{C_0} \times\ 100\% \tag{3}$$

where q_e: equilibrium adsorption capacity (mg/g), C_0: initial concentration (mg L^{-1}), C_e: equilibrium concentration (mg L^{-1}), m: weight of aerogel (mg), V: solution volume (mL) and R: removal efficiency (%).

Two conventional isotherm equations including the Freundlich (Eq. 4), and the Langmuir (Eq. 5) have been tested with the data sets [17].

$$q_e = K_F c_e^{\frac{1}{n}} \tag{4}$$

$$q_e = \frac{q_m K_L c_e}{1 + K_L c_e} \tag{5}$$

where K_F and n are Freundlich constants related to adsorption capacity and adsorption intensity, respectively; q_m and K_L are Langmuir constants and represent the maximum adsorption capacity of adsorbents (mg g^{-1}) and the energy of adsorption, respectively.

Results and Discussion

Optimization of the Preparation Parameters

In this experiment, the critical parameters involving the amount of glutaraldehyde and APTMS, modification temperature, and time, were optimized through the single-factor variable method to achieve the best adsorption performance, as shown in Fig. S2. Based on the detailed discussion in Text S1, it was suggested that the optimum synthesis condition was 1.5 mL of glutaraldehyde and 2 g of APTMS, and the mixture was reacted at 333 K for 4 h.

Table 1 Parameters of artificial synthesis electroplating wastewater

Ion	Ni^{2+}	Cr^{6+}	Zn^{2+}	Cu^{2+}	Fe^{3+}	Pb^{2+}	PO_4^{3-}	SO_4^{2-}
Conc. (mg L^{-1})	20	32	24	1.02	26	2.5	1.5	546

Characterization

The surface micromorphology of Fe_3O_4@CS and Fe_3O_4@CS-APTMS was characterized by SEM (Fig. 1) and TEM (Fig. S3). As shown in Fig. 1a and b, the Fe_3O_4 was coated and mostly immersed into the loose structure of CS to form numerous interconnected and stacked spheres at diameters around 50 to 230 nm. Compared with the samples of chitosan-coated cotton fiber composite, the particles synthesized in this study are larger and more irregular [30]. After the loading of the APTMS, the surface (Fig. 1c and d) was covered with more obvious folding and wrinkling, the degree of roughness and agglomeration increased, and the core-shell structure became inconspicuous. The possible reason for this phenomenon was that the load of APTMS and the cross-linking reaction introduced new molecular chains, altered the loose surface, and occupied the interior porous structure of Fe_3O_4@CS.

FTIR was utilized to investigate the variation of functional groups among CS, Fe_3O_4@CS, and Fe_3O_4@CS-APTMS, the results are shown in Fig. 2a. The characteristic peak of pristine CS at 2878 cm^{-1} can be attributed to the tensile vibration of C–H [22]. The peaks at 1653 and 1600 cm^{-1} are related to the stretching vibration of the amide I band (C=O) and amide II band (– NH_2) [17]. Broader absorption peaks at 3441 cm^{-1} corresponded to the stretching vibration of –NH_2 and–OH [31]. In addition, the bending vibration of –OH, C–O–C stretching, and C–O stretching vibration can be traced to the absorption peaks at 1388, 1153, and 1095 cm^{-1} [32]. Compared with raw CS, the new Fe–O vibration at 596 and 581 cm^{-1} confirmed the existence of Fe_3O_4 nanoparticles in Fe_3O_4@CS and Fe_3O_4@CS-APTMS [22]. The new peaks at 1664 cm^{-1} were related to the stretching vibration of the new C=N bond generated by the Schiff base reaction [33]. The peak of –NH_2 and–OH (3436 cm^{-1}) in Fe_3O_4@CS-APTMS was attributed to the incorporation of modified amino groups. Additionally, the new absorption peak

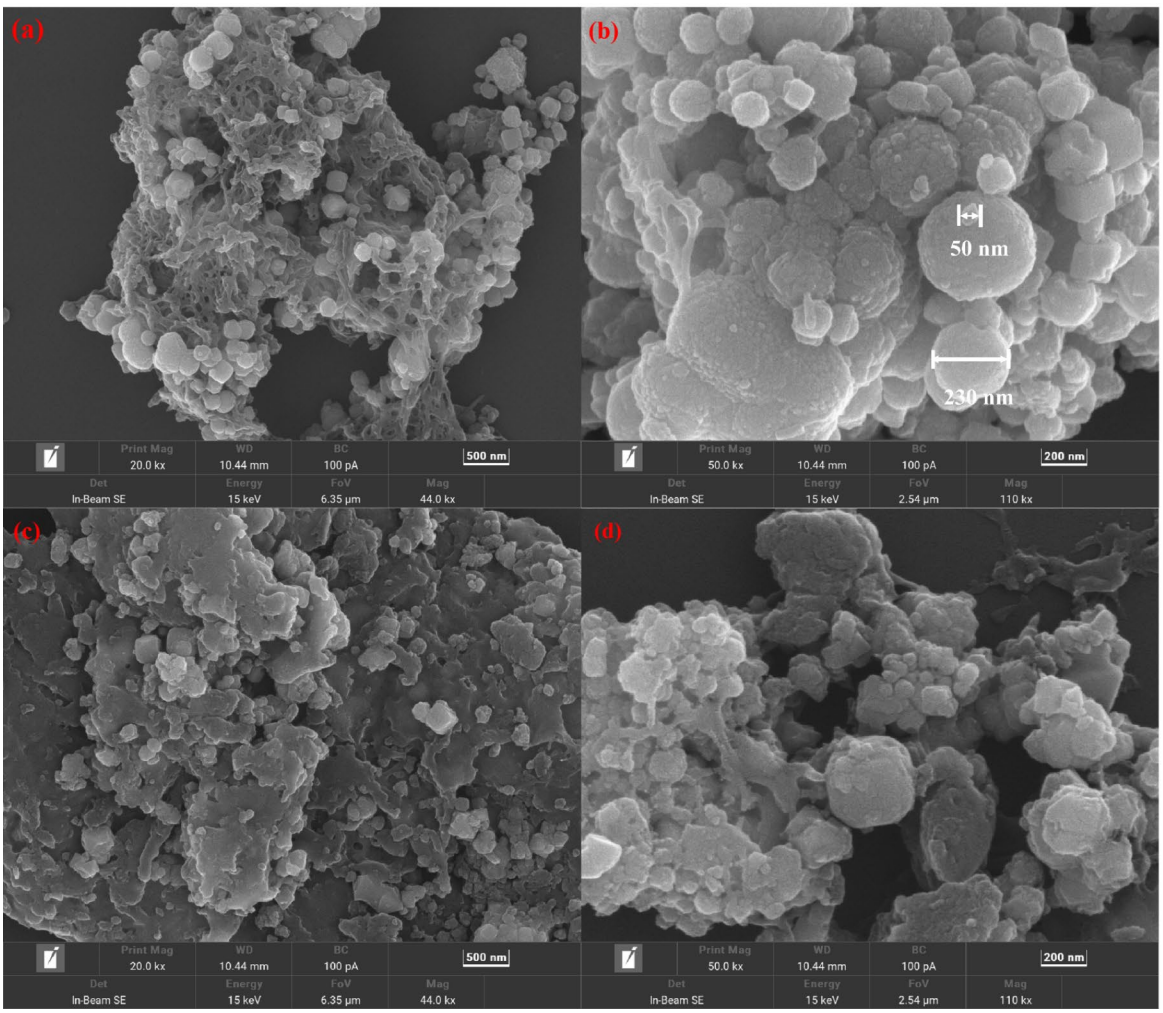

Fig. 1 Low-resolution (**a**) and high-resolution (**b**) SEM images of Fe_3O_4@CS, low-resolution (**c**), and high-resolution (**d**) SEM images of Fe_3O_4@CS-APTMS

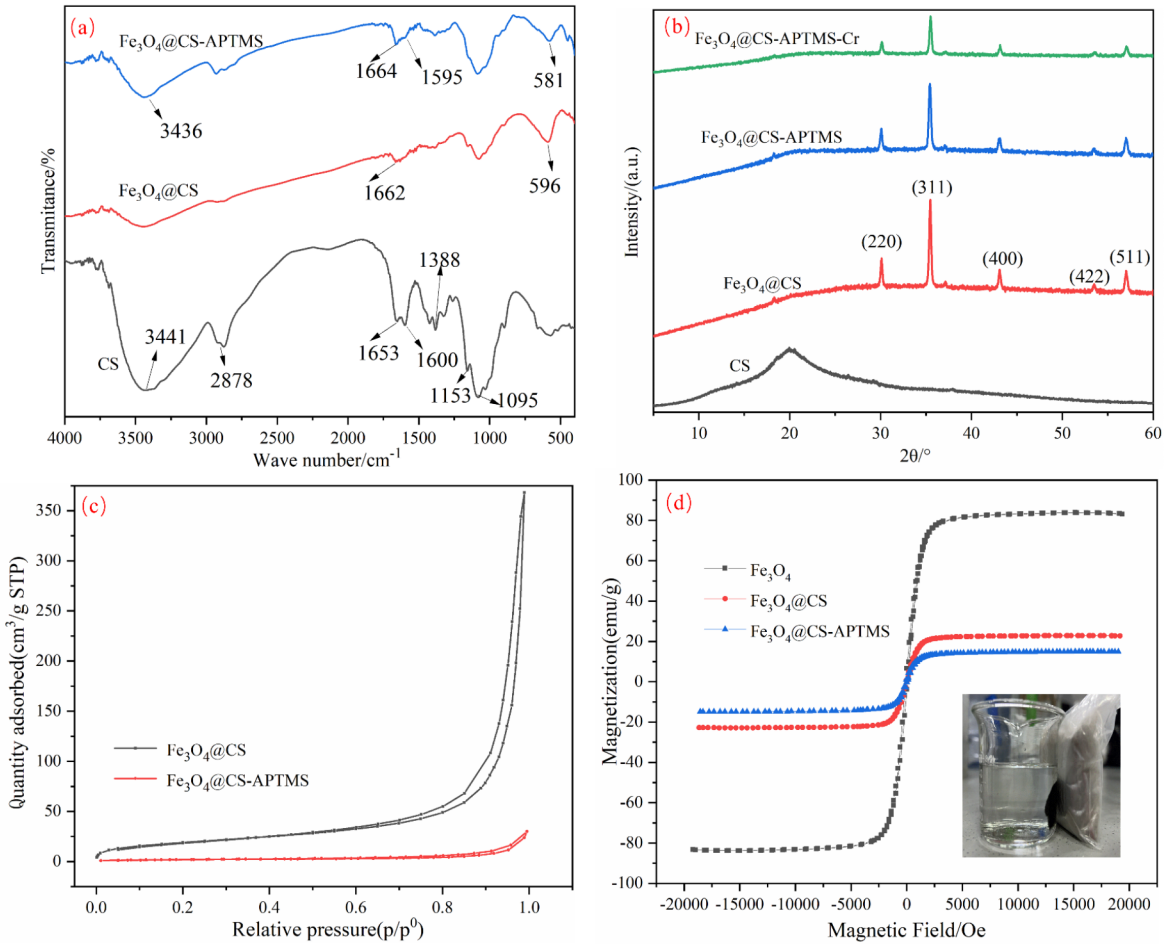

Fig. 2 FTIR spectrum of CS, Fe_3O_4@CS, and Fe_3O_4@CS-APTMS (**a**), XRD spectrum of CS, Fe_3O_4@CS, Fe_3O_4@CS-APTMS and Fe_3O_4@CS-APTMS-Cr (**b**), N_2 adsorption-desorption isotherm of Fe_3O_4@CS and Fe_3O_4@CS-APTMS (**c**), VSM spectrum of Fe_3O_4, Fe_3O_4@CS, and Fe_3O_4@CS-APTMS (**d**)

at 1595 cm^{-1} corresponded to the N–H deformation vibrations. These variations confirmed the successful synthesis of amino-modified magnetic CS composite. Furthermore, the amino content of the as-prepared composite before and after modification was determined by hydrochloric acid labeling titration, they were determined as 0.64 and 0.86 mmol g^{-1}, the elevated amino content, and the enhanced internal structure promoted the capacity to 1.34 times of that of Fe_3O_4@CS, and enabled the composite to trap Cr(VI) at pH 2, highlighting the decoration of functional groups.

The Fe_3O_4@CS-APTMS and Fe_3O_4@CS nanocomposites showed similar X-ray (Fig. 2b) diffraction patterns, namely 30.12°, 35.46°, 43.10°, 53.47°, and 57.04° assigned to the indices (220), (311), (400), (422), (511) [22]. The characteristic peaks of Fe_3O_4 still existed in both materials, indicating the crystal structure of Fe_3O_4 retained during the preparation process. As an amorphous chemical, CS exhibited a wide diffraction peak at 19.92° [17]. This peak was also discovered at spectra of Fe_3O_4@CS and Fe_3O_4@CS-APTMS, which indicated that CS was one of the components of the materials. Meanwhile, no other obvious changes in the peak were found, but intensity weakened after the successful modification by APTMS. These results were consistent with the FTIR findings, proving that the magnetic amino-modified composites were synthesized.

To better explore the physical properties of Fe_3O_4@CS and Fe_3O_4@CS-APTMS composites, Brunauer–Emmett–Teller (BET) was performed to characterize the specific surface area of the adsorbents. The N_2 adsorption-desorption isotherms were shown in Fig. 2c. The adsorption-desorption isotherms belonged to type IV since a closed hysteresis loop was found at the relative pressure P/P_0 of 0.4 ~ 1.0 indicating the existence of mesoporous structures [34]. The pore size and pore volume of Fe_3O_4@CS-APTMS in Table S1 decreased compared with unmodified Fe_3O_4@CS. The specific surface area of the modified composite decreased from 69.77 to 7.08 $m^2\ g^{-1}$, which may be because the APTMS was decorated inside the mesopore via cross-linking, blocking some of the pores of Fe_3O_4@CS. These phenomena on the decline of specific surface area and pore volume after functionalization were similar to previous studies for the same reason [34–36]. The adsorption capacity was not affected by the reduced specific surface area, conversely, it was significantly enhanced due to the successful introduction of amino-containing groups.

The magnetization hysteresis loops at room temperature were also characterized to detect magnetism. As shown in Fig. 2d, the saturation magnetization (M_s) of the pristine Fe_3O_4 particles was about 83.67 emu g^{-1}, which dramatically declined to 22.83 of Fe_3O_4@CS and 14.79 emu g^{-1} of Fe_3O_4@CS-APTMS, respectively. The decrease of M_s among the composite could be attributed to the coating of the polymer shell impairing the magnetic strength of Fe_3O_4. However, this composite material still exhibited strong magnetic responsiveness for rapid separation under the external magnetic field (Fig. 2d, inset), which was beneficial to the recovery performance.

The Removal Performance of Fe_3O_4@CS-APTMS

Effect of pH

One of the essential factors that affected the adsorption efficiency is the initial pH value of the solution, which influences the chemical potential and level of protonation of the adsorbent and determines the metal ions' physicochemical properties. The specific species distribution of Cr(VI) in water is one of the crucial factors affecting the adsorption process of Cr(VI). The pH plays a significant role in the adsorption process by changing the metal ion species and the (de)protonation of functional groups. Fig. S4 displays the distribution of Cr(VI) species across a pH range of 1 to 11. The Cr(VI) species was highly pH dependent, the H_2CrO_4, $HCrO_4^-$ and $Cr_2O_7^{2-}$ were the dominating species at pH < 5 [37]; whereas the concentration of $HCrO_4^-$ gradually declined, and that of CrO_4^{2-} fleetly increased at pH > 5, which later dominated at 8 < pH < 11 [38].

To determine the optimal pH for Cr(VI) removal, the adsorption performance of Fe_3O_4@CS-APTMS was investigated across a pH range of 1.0 to 11.0 (Fig. 3a). The removal rate increased at first and then decreased along with the pH augment, and reached the peak at pH 2.0. As we all know, the amino group protonation would be enhanced with pH decline from neutral to acidity, which facilitated Cr(VI) sorption via the electrostatic attraction. However, the efficiency suddenly decreased at 1.0, presumably due to Cr(VI) species conversion. To be more specific, more neutral H_2CrO_4 appeared at pH < 2.0, leading to the weakening in electrostatic attraction between the adsorbent and Cr(VI) [39]. It should be mentioned that the performance of Fe_3O_4@CS was not studied due to it was dissolved in an acidic condition (pH < 5). The reason for acid dissolution was that Fe_3O_4@CS was not chemically modified. In contrast, the APTMS-modified magnetic chitosan composites exhibited excellent acid resistance and adsorption capacity under acidic conditions.

To uncover the surface charge status of Fe_3O_4@CS-APTMS under different pH conditions, Zeta potential was measured and displayed in Fig. 3a, the surface of Fe_3O_4@CS-APTMS was protonated with relatively high positive potentials at pH < 4.3. The positively charged surface can favor the Cr(VI) adsorption by electrostatic attraction, leading to an enhanced capacity of Fe_3O_4@CS-APTMS. In contrast, the deprotonation effect results in the negatively charged surface of Fe_3O_4@CS-APTMS at pH > 4.3, causing an obstacle to the capturing of Cr(VI) due to the electrostatic repulsion [40]. The material exhibited the highest zeta potential (55.4 mV) and the maximum adsorption capacity at pH 2, suggesting that the most abundant surface positive charge was advantageous for Cr(VI) adsorption. Taking into account that the actual industrial wastewater, such as electroplating effluent, was acidic, pH 2.0 was selected as the optimal pH for the subsequent batch experiments.

Effect of Adsorbent Dosage

The fewer dosages with excellent performance would be beneficial to the cost saving, hence the impact of adsorbent dosage was an indispensable component to evaluate the application potential of the material. As shown in Fig. 3b, the adsorption capacity descended as the amounts of Fe_3O_4@CS-APTMS increased, whereas their removal rates sharply elevated and then tended to an equilibrium. The inverse relationship between capacity and removal rate could be explained by the fact that increasing the amount of adsorbent provides more accessible active sites, which reduces the Cr(VI) content and achieves higher efficiency. Nonetheless, adding a larger amount of the composite to a solution containing a fixed mass of Cr(VI) results in lower

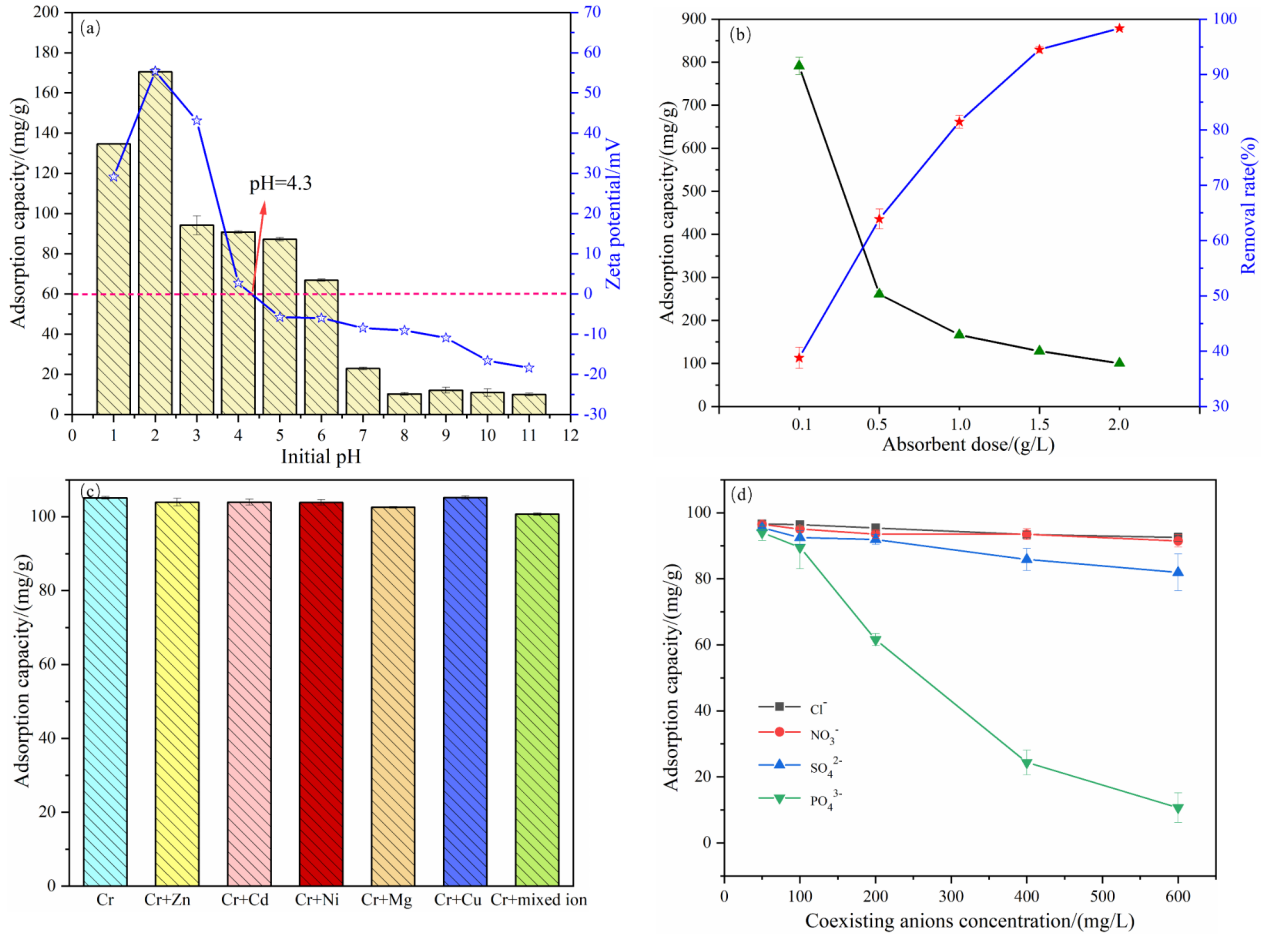

Fig. 3 The Cr(VI) adsorption performance and zeta potential of adsorbent at different pHs (C_0, 200 mg L^{-1}; dosage, 1 g L^{-1}, pH 2; reaction time, 720 min; T, 298 K) (**a**), the Cr(VI) adsorption performance under different dosages (C_0, 200 mg L^{-1}; dosage, 0.2 ~ 2 g L^{-1}; pH 2; reaction time, 720 min) (**b**), the effect of binary and multi-metals (Cr(VI) and co-existing cation concentration: 100 mg L^{-1}) (**c**) and co-existing anions(C_0, 100 mg L^{-1}; dosage, 1 g L^{-1}; pH 2; reaction time, 720 min) (**d**) on the Cr(VI) adsorption performance of the material

capacity. Although the cross point of the two curves was discovered near 0.5 g L^{-1}, the removal rate was not sufficient to purify the majority of the Cr(VI), so subsequent experiments selected the dosage at 1.0 g L^{-1} to achieve the removal rate and adsorption capacity as higher than 80% and 170 mg g^{-1}.

Effects of Ion Strength and Competing Cations

Wastewater contains tremendous other ions that forcefully compete with Cr(VI) for the adsorption sites on the fabricated Fe_3O_4@CS-APTMS. Figure 3c and d depict the impact of the selected ions including the cations (Ni^{2+}, Mg^{2+}, Cu^{2+}, Zn^{2+}, Cd^{2+}) and anions (Cl^-, NO_3^-, SO_4^{2-}, PO_4^{3-}) on the performance of Fe_3O_4@CS-APTMS. On the one hand, Fig. 3c shows that the adsorption capacities in both binary and multiple mixed metal solutions are comparable to the single fractions of Cr(VI). The presence of metal cations (Ni^{2+}, Mg^{2+}, Cu^{2+}, Zn^{2+}, Cd^{2+}) had minimal impact on the uptake of Cr(VI) because of the oppositely charged conditions, which demonstrated that Fe_3O_4@CS-APTMS was suitable for industrial wastewater treatment containing a variety of heavy metals. On the other hand, Fig. 3d shows that Cl^- and NO_3^- did not interfere with the Cr(VI) adsorption when the concentration was in the range of 0 to 600 mg L^{-1}. In contrast, the presence of SO_4^{2-} and PO_4^{3-} could produce an inhibitory effect: the capacity decreased from 91.86 to 81.92 mg g^{-1} when the SO_4^{2-} concentration increased from 200 to 600 mg L^{-1}, a much steeper decreasing trend (61.58 to 10.57 mg g^{-1}) was discovered as the concentration of PO_4^{3-} elevated. This phenomenon may be ascribed to the fact that multivalent anions SO_4^{2-} and PO_4^{3-} would possess

similar adsorption behaviors and occupy the analogical active sites. Another vital reason was that the ion energy and electrostatic adsorption of SO_4^{2-} (divalent anion) and PO_4^{3-} (trivalent anion) is stronger than that of monovalent ions such as Cl^- and NO_3^- [41], which has stronger competitiveness for the positive charge sites on the surface of Fe_3O_4@CS-APTMS, thereby weakening the adsorption of Cr(VI).

Adsorption Kinetics

The adsorption kinetic models involving the pseudo-first-order (PFO) and pseudo-second-order (PSO) models can be adopted to estimate the adsorption rate as well as reveal the potential mechanism of the reaction [42]. The experiments were carried out at 50 mg L^{-1}, 100 mg L^{-1}, and 500 mg L^{-1} Cr(VI) solution, their equilibrium reached within 60 min, 120 min, and 360 min with the capacity was 48.39 mg g^{-1}, 177.00 mg g^{-1}, and 295.58 mg g^{-1} (Fig. 4a), respectively. However, with the extension of contact time, the adsorption process became sluggish after reaching equilibrium at the distinct time depending on the initial content of Cr(VI).

The fitting result demonstrated that the PSO (Fig. 4c) model achieved a higher fitting coefficient ($R^2 = 0.999$) than that of PFO (Fig. 4b). By comparison, the PSO model was more suited to explain the Cr(VI) adsorption dynamics of Fe_3O_4@CS-APTMS because it presented the higher correlation coefficient R^2 in linear fitting results [43]. The fitting parameters shown in Table S2 present a higher adsorption rate constant k^2, which meant the adsorbent could quickly capture Cr(VI) at a low concentration. The maximum theoretical adsorption capacity ($q_{e,cal}$=296.74 mg g^{-1}) estimated from the PSO model was by the actual adsorption capacity ($q_{e,exp}$=296.60 mg g^{-1}). Thus, these results hinted that chemical adsorption was the primary factor in rate-limiting adsorption [44].

Adsorption Isotherms

Adsorption isotherms at different temperatures (298, 318, and 338 K) were used to figure out the interaction behaviors between Cr(VI) and Fe_3O_4@CS-APTMS. Herein, the most commonly used models such as the Langmuir and Freundlich [38] isotherm models have been employed as shown

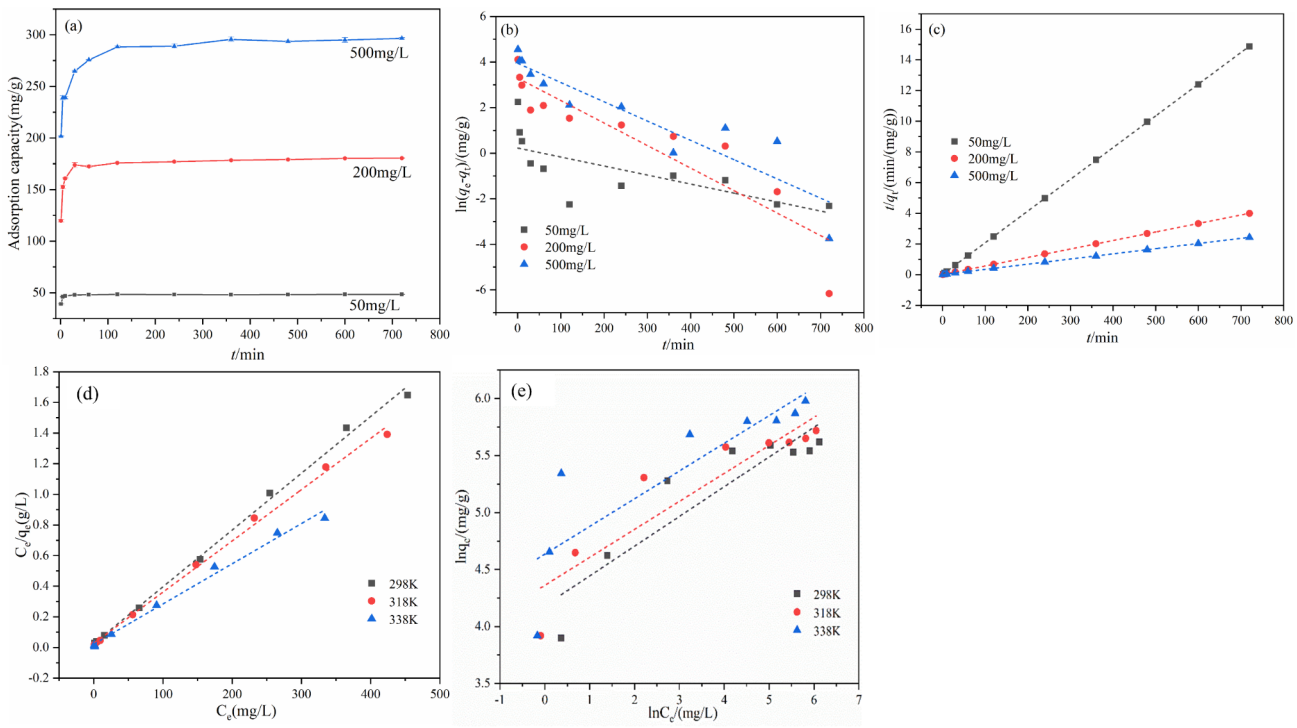

Fig. 4 Kinetic adsorption curves of Cr(VI) under three concentrations (**a**), the fitting curves of PFO model (**b**), and the right curves of PSO model (**c**), Langmuir (**d**) and Freundlich (**e**) isotherm fitting curves (C_0, 50 ~ 500 mg L^{-1}; pH 2; reaction time, 720 min)

in Fig. 4d and e. Table S3 lists the relevant parameters of the models. The determination coefficient in Table S3 of the Langmuir equation ($R^2 = 0.996$) was more appropriate than that of Freundlich ($R^2 = 0.836$). The results indicated that a monolayer coverage of target pollutants is adsorbed onto the homogenous surface of the Fe_3O_4@CS-APTMS [45]. Based on this, it is reasonable to conclude that the adsorption of Cr(VI) on Fe_3O_4@CS-APTMS was dominantly controlled by the monolayer adsorption via the chemical bonding. Notably, the maximum adsorption capacities were estimated to be 269.54 mg g^{-1}, 298.51 mg g^{-1}, and 380.22 mg g^{-1} at 298 K, 318 K, and 338 K, respectively. The actual adsorption capacities were 254.72, 284.5, and 354.53 mg g^{-1} respectively. Compared with previously reported magnetic adsorbents anchored amino-functional group (Table S4), the adsorption properties of Fe_3O_4@CS-APTMS composite emerged as an outstanding material. Compared with other mesoporous materials, it also has advantages in adsorption capacity [46–51]. Therefore, Fe_3O_4@CS-APTMS is indeed a class of promising adsorbents for the removal of Cr(VI) from the water environment.

Temperature affects the diffusion of Cr(VI) on the material surface and within the pore structure during adsorption, affecting the adsorption performance [52]. Hence, the adsorption capacity of Cr(VI) increased from 183.16 to 196.08 mg g^{-1} as the adsorption temperature rose from 298 to 338 K (Fig. S5a). The elevated temperature could highly promote intermolecular movement, and accelerate the movement and the binding of Cr(VI) to the amino group of Fe_3O_4@CS-APTMS. Moreover, the adsorption data were fitted by Van't Hoff Equation (Fig. S5b) to calculate the relevant parameters in Table S5. The negative ΔG^{θ} values indicated that Cr(VI) sorption on Fe_3O_4@CS-APTMS was thermodynamically spontaneous, while the positive ΔH^{θ} and ΔS values revealed that the sorption was an endothermal and entropic process [17]. These results confirmed that of those amino-modified composites: the binding of Cr(VI) and the amino group was promoted by the higher temperature.

Reusability

The reusability of the material is essential for adsorbents from a practical and economic point of view, hence the five adsorption-desorption cycles were carried out. As depicted in Fig. S6, the removal rates of Cr(VI) by Fe_3O_4@CS-APTMS remained above 90% during the five regeneration cycles. More importantly, the 0.01 mol L^{-1} NaOH could achieve elution efficiencies of 80% during the desorption process, which could be attributed to the strong deprotonation of N groups in the adsorption active sites caused by the strong alkalinity of the desorption agent. Afterward, the Fe_3O_4@CS-APTMS could be regenerated to achieve the sustained high capacity for Cr(VI) to save the cost. Consequently, Fe_3O_4@CS-APTMS was a promising candidate for the removal of aqueous Cr(VI) in real application.

Application in Artificial Electroplating Wastewater

The strict control of hexavalent chromium emissions has become an international trend. The national emission standard for pollutants in the electroplating industry in China restricted the concentration of Cr(VI) should not exceed 0.2 mg L^{-1}. The artificial electroplating wastewater was prepared according to the parameters of industrial electroplating wastewater [29], which the parameters are shown in Table 1. After treatment, the total removal rate exceeded 99.70% at 1 g L^{-1} of the adsorbent, and the Cr(VI) concentration was reduced from 32 to 0.09 mg L^{-1}, which was far below the requirement of the relevant national standard. The results confirmed forcefully the substantial application potential of Fe_3O_4@CS-APTMS for Cr(VI) removal from actual industrial wastewater.

Adsorption Mechanism

XPS spectra were generally used to detect the existence of a particular element and to identify its possible species since the electron configuration of the atom would be modified by the change of chemical bonds. The full-scan XPS spectrum of Fe_3O_4@CS-APTMS is shown in Fig. 5a, the peaks of C1s, N1s, O1s, Si2p, and Fe2p were distributed at 285.08, 400.08, 532.08, 102.08, and 975.08 eV, respectively. After adsorption, the peak involving Cr2p newly appeared at 578.08 eV, specifically, the new peaks appeared (Fig. 5b) at around 576.54 and 586.33 eV of Fe_3O_4@CS-APTMS-Cr were attributed to $Cr2p_{3/2}$ and $Cr2p_{1/2}$, which indicated the successful sorption of Cr onto Fe_3O_4@CS-APTMS. The peaks at 576.47 eV ($Cr2p_{3/2}$) and 585.98 eV ($Cr2p_{1/2}$) were related to Cr(III), while the peaks at 578.67 eV ($Cr2p_{3/2}$) and 587.34 eV ($Cr2p_{1/2}$) corresponded to Cr(VI). The peak area ratios of Cr(VI) and Cr(III) were 35% and 65%, respectively. These results demonstrated that both Cr(VI) and Cr(III) were uptake on the Fe_3O_4@CS-APTMS. The presence of Cr(III) directly demonstrated that a portion of Cr(VI) has been successfully reduced to Cr(III) and subsequently absorbed onto the material's surface. After the adsorption reached the equilibrium in the Cr(VI) solution with an initial concentration of 120.19 mg L^{-1}, the aquatic Cr(III) was measured to be 6.34 mg L^{-1} in the treated water. Combined with the above-mentioned XPS analysis indicated, Fe_3O_4@CS-APTMS can effectively adsorb and reduce Cr(VI) by hydroxyl and amino groups while becoming immobilized on the material's surface as Cr(III) at nearly 67.15% of the initial amount.

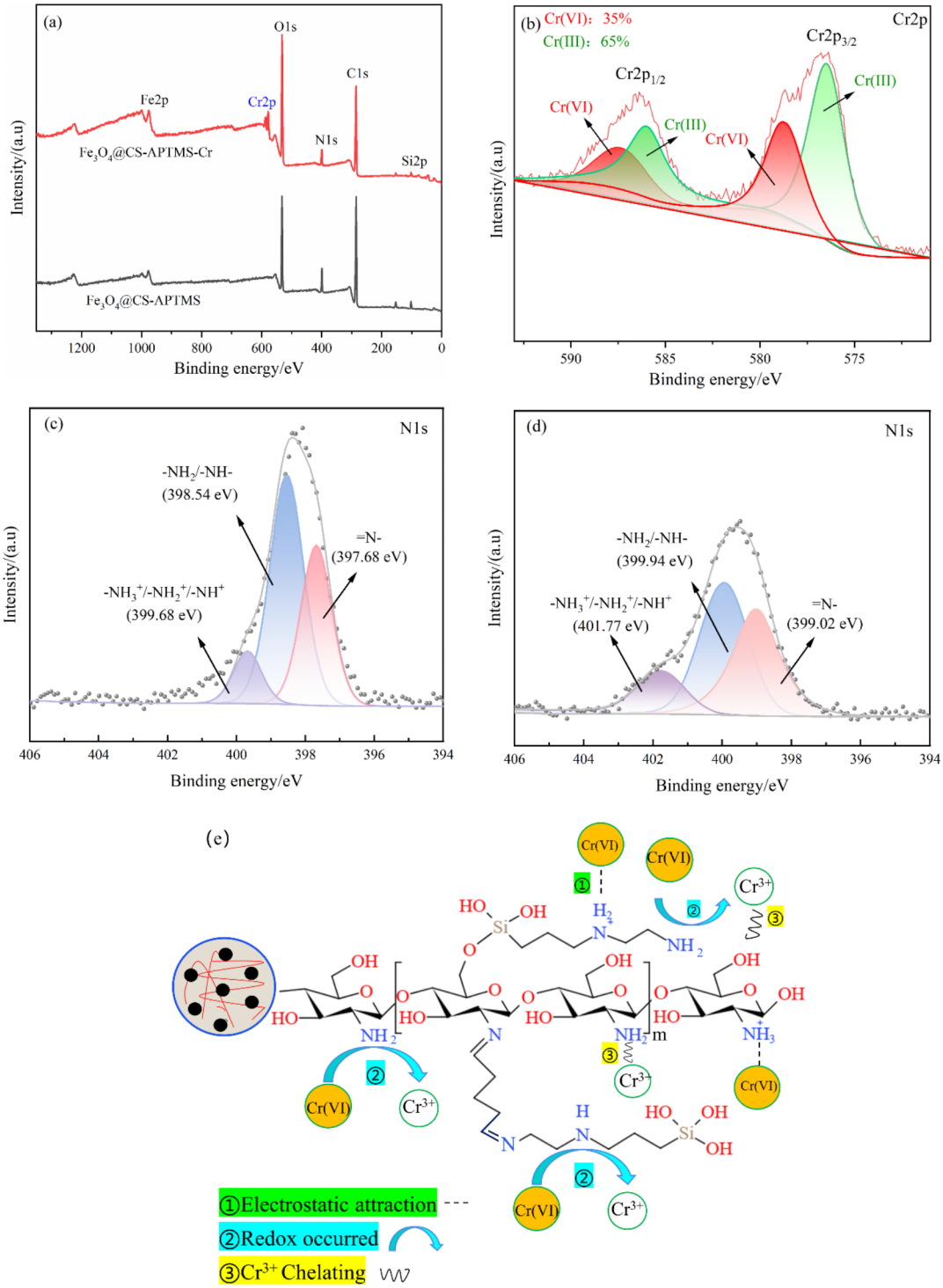

Fig. 5 XPS full scan spectra of Fe_3O_4@CS-APTMS and Fe_3O_4@CS-APTMS-Cr (**a**); the high-resolution spectrum of Cr2p of Fe_3O_4@CS-APTMS-Cr (**b**); N1s of Fe_3O_4@CS-APTMS (**c**) and Fe_3O_4@CS-APTMS-Cr (**d**), removal mechanism of Cr(VI) (**e**)

The high-resolution spectra of N1 s before and after adsorption are depicted in Fig. 5c and d. Before adsorption, the peaks at 399.68, 398.54, and 397.68 eV could be ascribed to the protonated amine group ($–NH_3^+$/$–NH_2^+$/$–NH^+$), free amino groups (–NH_2/–NH–) and imine (=N–), respectively [40]. After Cr(VI) adsorption, the only variation was that they shifted to higher binding energy, which confirmed that there was a strong interaction between the nitrogen-containing functional group and Cr. The peak ratio of $–NH_3^+$/$–NH_2^+$/$–NH^+$ increased and the peak ratio of –NH_2/–NH– decreased significantly after Cr(VI) loading, which once again proved that the amino group played a major role in the adsorption and reduction of Cr(VI) [53]. Based on the above-mentioned analyses, a possible mechanism for the Cr(VI) removal by Fe_3O_4@CS-APTMS was proposed (Fig. 5e) from two aspects involving adsorption and reduction: once the adsorbent was added into the Cr-containing wastewater at pH 2.0, the efficient groups on Fe_3O_4@CS-APTMS, e.g. =N–, NH, and–NH_2, were rapidly protonated to $–NH^+$/$–NH_2^+$/$–NH_3^+$, and the electronegative Cr(VI) species ($HCrO_4^-$) were adsorbed onto the composite surface via electrostatic attraction. Whereafter, they were partly reduced to Cr(III) by the amino groups [38]. The majority of Cr(III) was immobilized onto Fe_3O_4@CS-APTMS through chelation with the nitrogen/oxygen on the adsorbent, and only a handful of Cr(III) (6.34 mg L^{-1}) was leaked into the bulk solution [53].

For the established conclusions, DFT calculation (Fig. 6a–d) was further exploited to elucidate their rationality. The optimized structure of Fe_3O_4@CS-APTMS and the composite structures after adsorption were illustrated in Fig. 6a. The predominant species were identified as $HCrO_4^-$, which were adsorbed on CS-APTMS via electrostatic interaction of protonated amine groups (NH_3^+) with a high interaction energy of − 12.181 eV (Fig. 6b), respectively. Accordingly, it could be concluded that the adsorption behavior of Cr(VI) ions by Fe_3O_4@CS-APTMS was feasible. The adsorption energies for the binding of Cr(III) to the amino (Fig. 6c) and hydroxyl group (Fig. 6d) were − 2.189 and − 7.992 eV, respectively. Consequently, the majority of Cr(III) was immobilized onto Fe_3O_4@CS-APTMS through chelation with the amino and hydroxyl groups on the adsorbent, and only a handful of Cr(III) (6.34 mg L^{-1}) was leaked into the bulk solution [53]. The production Cr(III) would be dissolved into the bulk solution due to its high solubility. However, the XPS analysis revealed that the Cr(III) loaded on the material occupied 65%, while the interaction energy of the Cr(III) amino (− 2.189 eV) was extremely lower than that of $HCrO_4^-$ amino, hence it was proved that the anionic Cr(VI) was firstly bonded to the amino group; Subsequently, a portion of the adsorbed Cr(VI) ions participated in a reduction reaction with amin.

Conclusions

In summary, Fe_3O_4@CS-APTMS composites were developed via a facile method with the Schiff base reaction and cross-linking strategy for the removal of Cr(VI) in simulated electroplating wastewater. The SEM, TEM, and BET results demonstrated that APTMS grafting and the cross-linking reaction covered the Fe_3O_4@CS-APTMS surface with more obvious folding and wrinkling and blocked the interior pores. After being modified by APTMS, the CS can be prevented from dissolving in acid water and has more amino groups to adsorbed Cr(VI). The maximum adsorption capacity reached 269.54 mg g^{-1} at 298 K, which was significantly higher than that of most CS-based adsorbents previously reported. Both the adsorption kinetics and the isotherm of Cr(VI) can be accurately described using the pseudo-second-order kinetic model and the Langmuir model, respectively. XPS analysis and DFT theoretical calculations have confirmed that the superior performance was attributed to electrostatic attraction, reduction, and chelation. The redox reaction originating from –NH/–NH_2 participated in the Cr(VI) detoxification, and partial Cr(III) was trapped on the composite by hydroxyl and amino groups. Although the material could achieve high performance in acidic wastewater, the removal effect at pH neutral and alkaline was poor, which still needs to be further explored. The as-prepared Fe_3O_4@CS-APTMS composites could be applied as a potential, and efficient material for Cr(VI) remediation in electroplating wastewater, while minimizing the release risks to the treated water.

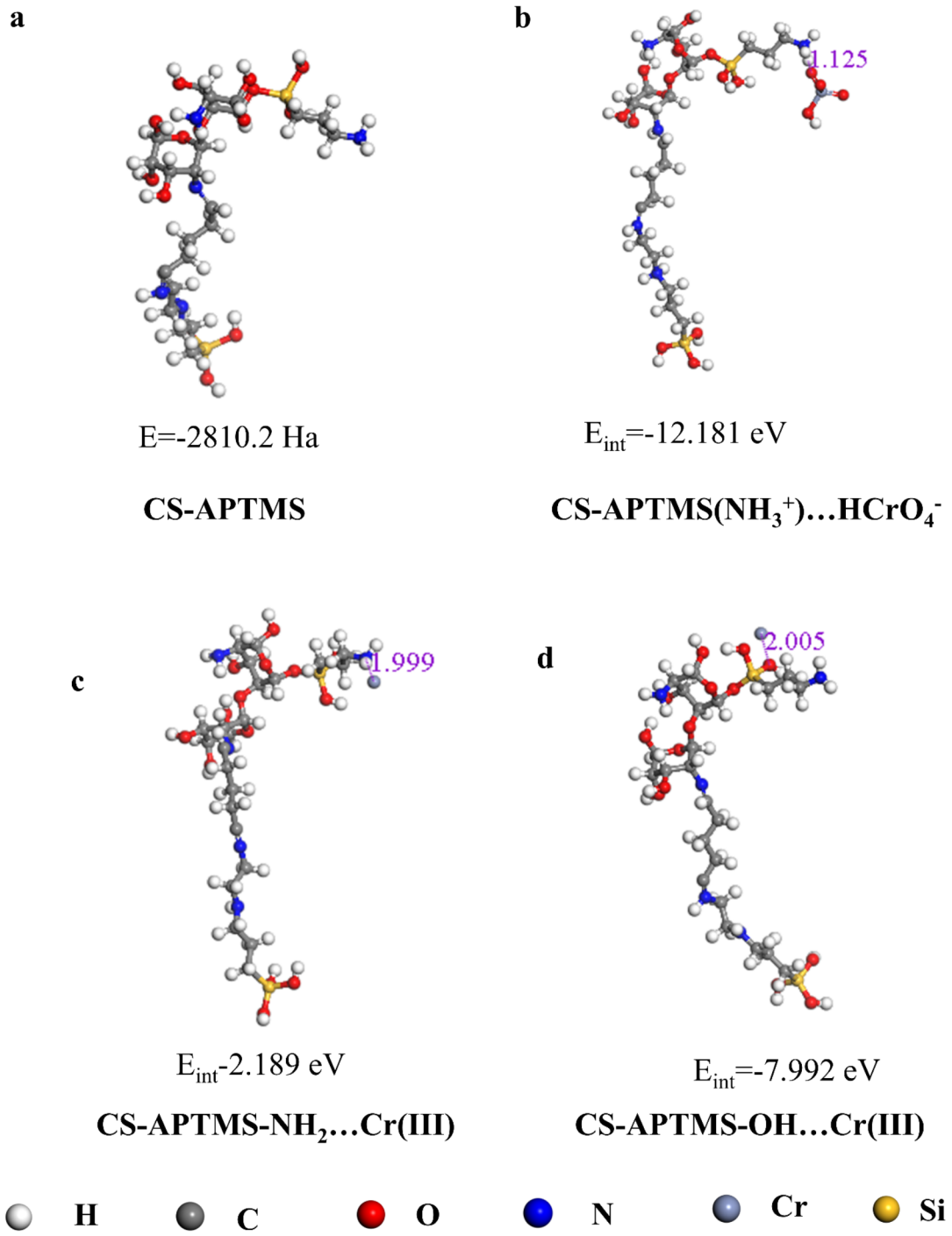

Fig. 6 The optimized geometries of CS-APTMS (**a**), CS-APTMS(NH_3^+) ⋯ $HCrO_4^-$ (**b**), CS-APTMS-NH_2 ⋯ Cr(III) (**c**) and CS-APTMS-OH ⋯ Cr(III) (**d**). (The C, N, O, H, Cr, and Si are represented by gray, blue, red, white, blue–gray, and yellow, respectively)

Supplementary Information The online version contains supplementary material available at https://doi.org/10.1007/s10924-024-03390-7.

Author Contributions Lixin Huang: Conceptualization, Methodology, Resources, Formal analysis, Writing—review & editing. Mingen Li: Conceptualization, Methodology, Validation, Investigation. Haiying Lin: Conceptualization, Writing review & editing, Supervision, Project administration, Funding acquisition. Qingge Feng: Conceptualization, Resources, Supervision. Qiuyan Hu: Conceptualization, Methodology, Investigation. Zixuan Chen: Investigation. Jiatong Lv: Conceptualization, Resources, Supervision. Jia Lin: Investigation. Lianghong Li: Investigation. Xianghua Wu: Investigation.

Funding The authors acknowledge the financial support from the National Natural Science Foundation of China (22166006), and Guangxi Natural Science Foundation (2020GXNSFAA297011).

Data Availability The data will be available upon request from the corresponding author.

Declarations

Competing Interests The authors declare that they have no known competing financial interests or personal relationships that could have appeared to influence the work reported in this paper.

References

1. Mokarram M, Saber A, Sheykhi V (2020) Effects of heavy metal contamination on river water quality due to release of industrial effluents. J Clean Prod 277:123380. https://doi.org/10.1016/j.jclepro.2020.123380
2. Lü T, Ma R, Ke K et al (2021) Synthesis of gallic acid functionalized magnetic hydrogel beads for enhanced synergistic reduction and adsorption of aqueous chromium. Chem Eng J 408:127327. https://doi.org/10/gr8bjn
3. Niu J, Ding P, Jia X et al (2019) Study of the properties and mechanism of deep reduction and efficient adsorption of cr(VI) by low-cost Fe_3O_4-modified ceramsite. Sci Total Environ 688:994–1004. https://doi.org/10.1016/j.scitotenv.2019.06.333
4. Huang Y, Wang B, Lv J et al (2022) Facile synthesis of sodium lignosulfonate/polyethyleneimine/sodium alginate beads with ultra-high adsorption capacity for cr(VI) removal from water. J Hazard Mater 436:129270. https://doi.org/10/grnnd3
5. Awual MR (2019) Novel ligand functionalized composite material for efficient copper(II) capturing from wastewater sample. Compos Part B Eng 172:387–396. https://doi.org/10.1016/j.compositesb.2019.05.103
6. Awual MR, Hasan MM, Iqbal J et al (2020) Naked-eye lead(II) capturing from contaminated water using innovative large-pore facial composite materials. Microchem J 154:104585. https://doi.org/10.1016/j.microc.2019.104585
7. Huang Y, Zeng X, Guo L et al (2018) Heavy metal ion removal of wastewater by zeolite-imidazolate frameworks. Sep Purif Technol 194:462–469. https://doi.org/10/gc375k
8. Yadav VB, Gadi R, Kalra S (2019) Clay based nanocomposites for removal of heavy metals from water: a review. J Environ Manag 232:803–817
9. Kyzas GZ, Bomis G, Kosheleva RI et al (2019) Nanobubbles effect on heavy metal ions adsorption by activated carbon. Chem Eng J 356:91–97
10. Awual MR, Hasan MM (2019) A ligand based innovative composite material for selective lead(II) capturing from wastewater. J Mol Liq 294:111679. https://doi.org/10.1016/j.molliq.2019.111679
11. Hossain MS, Shenashen MA, Awual ME et al (2024) Benign separation, adsorption, and recovery of rare-earth yb(III) ions with specific ligand-based composite adsorbent. Process Saf Environ Prot 185:367–374. https://doi.org/10.1016/j.psep.2024.03.026
12. Awual MR, Rahman IMM, Yaita T et al (2014) pH dependent cu(II) and pd(II) ions detection and removal from aqueous media by an efficient mesoporous adsorbent. Chem Eng J 236:100–109. https://doi.org/10.1016/j.cej.2013.09.083
13. Rasee AI, Awual E, Rehan AI et al (2023) Efficient separation, adsorption, and recovery of samarium(III) ions using novel ligand-based composite adsorbent. Surf Interfaces 41:103276. https://doi.org/10.1016/j.surfin.2023.103276
14. Sheikh MC, Hasan MM, Hasan MN et al (2023) Toxic cadmium(II) monitoring and removal from aqueous solution using ligand-based facial composite adsorbent. J Mol Liq 389:122854. https://doi.org/10.1016/j.molliq.2023.122854
15. Rehan AI, Rasee AI, Awual ME et al (2023) Improving toxic dye removal and remediation using novel nanocomposite fibrous adsorbent. Colloids Surf Physicochem Eng Asp 673:131859. https://doi.org/10.1016/j.colsurfa.2023.131859
16. Kubra KT, Hasan MM, Hasan MN et al (2023) The heavy lanthanide of thulium(III) separation and recovery using specific ligand-based facial composite adsorbent. Colloids Surf Physicochem Eng Asp 667:131415. https://doi.org/10.1016/j.colsurfa.2023.131415
17. Liu Y, Shan H, Pang Y et al (2023) Iron modified chitosan/coconut shell activated carbon composite beads for cr(VI) removal from aqueous solution. Int J Biol Macromol 224:156–169. https://doi.org/10.1016/j.ijbiomac.2022.10.112
18. Aydın YA, Aksoy ND (2009) Adsorption of chromium on chitosan: optimization, kinetics and thermodynamics. Chem Eng J 151:188–194. https://doi.org/10.1016/j.cej.2009.02.010
19. Vakili M, Rafatullah M, Salamatinia B et al (2014) Application of chitosan and its derivatives as adsorbents for dye removal from water and wastewater: a review. Carbohydr Polym 113:115–130
20. Bhatt R, Sreedhar B, Padmaja P (2015) Adsorption of chromium from aqueous solutions using crosslinked chitosan–diethylenetriaminepentaacetic acid. Int J Biol Macromol 74:458–466. https://doi.org/10/f65mtz
21. Khalil TE, Abdel-Salam AH, Mohamed LA et al (2023) Cross-linked modified chitosan biopolymer for enhanced removal of toxic Cr(VI) from aqueous solution. Int J Biol Macromol 234:123719
22. Zhang M, Zhang Z, Peng Y et al (2020) Novel cationic polymer modified magnetic chitosan beads for efficient adsorption of heavy metals and dyes over a wide pH range. Int J Biol Macromol 156:289–301. https://doi.org/10.1016/j.ijbiomac.2020.04.020
23. Awual MR, Alharthi NH, Hasan MM et al (2017) Inorganic-organic based novel nano-conjugate material for effective cobalt(II) ions capturing from wastewater. Chem Eng J 324:130–139. https://doi.org/10.1016/j.cej.2017.05.026
24. Waliullah RM, Rehan AI, Awual ME et al (2023) Optimization of toxic dye removal from contaminated water using chitosan-grafted novel nanocomposite adsorbent. J Mol Liq 388:122763. https://doi.org/10.1016/j.molliq.2023.122763
25. Awual MR, Islam A, Hasan MM et al (2019) Introducing an alternate conjugated material for enhanced lead(II) capturing from wastewater. J Clean Prod 224:920–929. https://doi.org/10.1016/j.jclepro.2019.03.241
26. Kubra KT, Salman MS, Hasan MN et al (2021) Utilizing an alternative composite material for effective copper(II) ion capturing from wastewater. J Mol Liq 336:116325. https://doi.org/10.1016/j.molliq.2021.116325

27. Li R, An Q-D, Mao B-Q et al (2017) PDA-meditated green synthesis of amino-modified, multifunctional magnetic hollow composites for cr(VI) efficient removal. J Taiwan Inst Chem Eng 80:596–606. https://doi.org/10.1016/j.jtice.2017.08.036
28. Liu W, Huang F, Wang Y et al (2011) Recycling $MgOH_2$ nanoadsorbent during treating the low concentration of cr(VI). Environ Sci Technol 45:1955–1961. https://doi.org/10.1021/es1035199
29. Mahmoud MR, Lazaridis NK (2015) Simultaneous removal of nickel(II) and chromium(VI) from aqueous solutions and simulated wastewaters by foam separation. Sep Sci Technol 50:1421–1432
30. Md. SS, Md. CS, Md. MH et al (2023) Chitosan-coated cotton fiber composite for efficient toxic dye encapsulation from aqueous media. Appl Surf Sci 622:157008. https://doi.org/10.1016/j.apsusc.2023.157008
31. Xu C, Xu Y, Zhong D et al (2023) Zr^{4+} and glutaraldehyde cross-linked polyethyleneimine functionalized chitosan composite: synthesis, characterization, cr(VI) adsorption performance, mechanism and regeneration. Int J Biol Macromol 239:124266
32. Mahfouz MG, Galhoum AA, Gomaa NA et al (2015) Uranium extraction using magnetic nano-based particles of diethylenetriamine-functionalized chitosan: equilibrium and kinetic studies. Chem Eng J 262:198–209
33. Han S, Zhou X, Xie H et al (2022) Chitosan-based composite microspheres for treatment of hexavalent chromium and EBBR from aqueous solution. Chemosphere 305:135486. https://doi.org/10/gq2rn9
34. Md RA, Md. NH, Md MH et al (2023) Green and robust adsorption and recovery of europium(III) with a mechanism using hybrid donor conjugate materials. Sep Purif Technol 319:124088. https://doi.org/10.1016/j.seppur.2023.124088
35. Salman MS, Hasan MN, Hasan MM et al (2023) Improving copper(II) ion detection and adsorption from wastewater by the ligand-functionalized composite adsorbent. J Mol Struct 1282:135259. https://doi.org/10.1016/j.molstruc.2023.135259
36. Hasan MM, Kubra KT, Hasan MN et al (2023) Sustainable ligand-modified based composite material for the selective and effective cadmium(II) capturing from wastewater. J Mol Liq 371:121125. https://doi.org/10.1016/j.molliq.2022.121125
37. Huang X, Hou X, Song F et al (2016) Facet-dependent cr(VI) adsorption of hematite nanocrystals. Environ Sci Technol 50:1964–1972. https://doi.org/10/f3rdzp
38. Liang X, Fan X, Li R et al (2018) Efficient removal of cr(VI) from water by quaternized chitin/branched polyethylenimine biosorbent with hierarchical pore structure. Bioresour Technol 250:178–184. https://doi.org/10.1016/j.biortech.2017.10.071
39. Pang Y, Zeng G, Tang L et al (2011) Preparation and application of stability enhanced magnetic nanoparticles for rapid removal of Cr(VI). Chem Eng J 175:222–227
40. Guo D-M, An Q-D, Xiao Z-Y et al (2018) Efficient removal of Pb(II), Cr(VI) and organic dyes by polydopamine modified chitosan aerogels. Carbohydr Polym 202:306–314
41. Huang Y, Lee X, Macazo FC et al (2018) Fast and efficient removal of chromium (VI) anionic species by a reusable chitosan-modified multi-walled carbon nanotube composite. Chem Eng J 339:259–267. https://doi.org/10.1016/j.cej.2018.01.133
42. Bulin C, Guo T, Zheng R, Xiong Q (2024) Interaction mechanism of phytic acid functionalized graphene oxide with ionic dyes. Sep Purif Technol 330:125369. https://doi.org/10.1016/j.seppur.2023.125369
43. Bulin C (2023) Adsorption mechanism and removal efficiency of magnetic graphene oxide-chitosan hybrid on aqueous Zn(II). Int J Biol Macromol 241:124588. https://doi.org/10.1016/j.ijbiomac.2023.124588
44. Liu F, Hua S, Hu Q et al (2022) Investigating the adsorption behavior and mechanism of Eu(III) and au(III) on β-cyclodextrin/polyethylenimine functionalized waste paper. Cellulose 29:1807–1820. https://doi.org/10.1007/s10570-021-04389-2
45. Liu F, Zhang Y, Wang S et al (2023) Elimination mechanisms of U(VI) and Se(IV) by MBenes supported Fe_3S_4 micro-crystal: synergy of adsorption, reduction and transformation. Appl Surf Sci 636:157813. https://doi.org/10.1016/j.apsusc.2023.157813
46. Awual MR (2016) Assessing of lead(III) capturing from contaminated wastewater using ligand doped conjugate adsorbent. Chem Eng J 289:65–73. https://doi.org/10.1016/j.cej.2015.12.078
47. Hasan MN, Salman MS, Islam A et al (2021) Sustainable composite sensor material for optical cadmium(II) monitoring and capturing from wastewater. Microchem J 161:105800. https://doi.org/10.1016/j.microc.2020.105800
48. Awual MR (2015) A novel facial composite adsorbent for enhanced copper(II) detection and removal from wastewater. Chem Eng J 266:368–375. https://doi.org/10.1016/j.cej.2014.12.094
49. Awual MR (2019) A facile composite material for enhanced cadmium(II) ion capturing from wastewater. J Environ Chem Eng 7:103378. https://doi.org/10.1016/j.jece.2019.103378
50. Awual MR (2017) Novel nanocomposite materials for efficient and selective mercury ions capturing from wastewater. Chem Eng J 307:456–465
51. Awual MR, Hasan MM, Khaleque MA, Sheikh MC (2016) Treatment of copper(II) containing wastewater by a newly developed ligand based facial conjugate materials. Chem Eng J 288:368–376. https://doi.org/10.1016/j.cej.2015.11.108
52. Liu F, Huang W, Wang S, Hu B (2022) Investigation of adsorption properties and mechanism of uranium(VI) and europium(III) on magnetic amidoxime-functionalized MCM-41. Appl Surf Sci 594:153376. https://doi.org/10.1016/j.apsusc.2022.153376
53. Zhang Y, Wen J, Zhou Y et al (2023) Novel efficient capture of hexavalent chromium by polyethyleneimine/amyloid fibrils/polyvinyl alcohol aerogel beads: functional design, applicability, and mechanisms. J Hazard Mater 458:132017. https://doi.org/10.1016/j.jhazmat.2023.132017